Available online at www.sciencedirect.com

SciVerse ScienceDirect

Ceramics International 38 (2012) 3781–3790

CERAMICS INTERNATIONAL

www.elsevier.com/locate/ceramint

Role of MgO on the HAp forming ability in phosphate based glasses

G. Rajkumar [a], V. Rajendran [b,*], S. Aravindan [c]

[a] Department of Physics, Kamaraj College of Engineering and Technology, Virudhunagar 626 001, Tamil Nadu, India
[b] Centre for Nano Science and Technology, K.S. Rangasamy College of Technology, Tiruchengode 637215, Tamil Nadu, India
[c] Department of Physics, Govt. Arts College, Salem 636 007, Tamil Nadu, India

Received 14 September 2011; received in revised form 7 January 2012; accepted 10 January 2012
Available online 1 February 2012

Abstract

Phosphate-based glasses $45P_2O_5$–30CaO–$(25-x)Na_2O$–xMgO for different compositions of $x = 0, 1, 2.5, 5$ and 10 mol% were prepared using the normal melt quench technique. To study the influence of MgO on phosphate glasses, a series of experimental analyses such as ultrasonic velocities, differential thermal analysis, X-ray diffraction, energy-dispersive X-ray spectroscopy, pH measurements, Fourier transform infrared spectroscopy, scanning electron microscopy and *in vitro* studies were carried out in all the prepared glasses. A maxima in ultrasonic parameters at $x = 2.5$ mol% of MgO content and a further decrease in the same with the addition of MgO content were observed in all glasses. The observed results indicate that structural compactness of glass network took place up to 2.5 mol% of MgO (PCNM2.5), beyond which a loose packing of atoms led to structural softening in glass network. The results obtained from X-ray diffraction, Fourier transform infrared spectroscopy and scanning electron microscopy analyses in all glasses before and after *in vitro* studies revealed the existence of higher HAp-forming ability in PCNM2.5 glass.

Keywords: Phosphate glasses; HAp; SBF; *In vitro*; Bioactive

1. Introduction

In recent years, silica-based bioactive glasses and glass ceramics have been developed for surgical implants [1]. Even though these glasses have several potential applications, their less-soluble nature makes them too hard to be compatible with biological tissues. The dissolution rate of silicon from bioglass is slow when compared with the body's ability to remove silicon through kidney filtration [2]. However, the long-term reaction of silica, both locally and systematically, is still unknown [3]. It is interesting to note that silica-free phosphate glasses show good biocompatibility because of their chemical composition, which is closer to the inorganic phase of natural bone [4,5]. Phosphate-based bioactive glasses have shown their identity in the field of biomaterials because of their tailor-made solubility with low melting, low glass transition and low softening temperatures [6]. The addition of a modifier oxide to the phosphate glass system increases the non-bridging oxygens (NBOs) in the glass network [7]. The presence of NBOs in the glass network is important in determining the solubility of glasses. Recently, there has been more focus on the development of new bioactive glasses for different applications by exploring the bioactivity of different compositions of glasses and glass ceramics [8–11].

The successful implantations of bioactive glasses for the replacement of damaged or diseased body parts have been shown extensively [12–18]. More attention has been paid to improve both bioactivity and mechanical strength of glasses by adding metal oxides to base glass [11,19–21]. The role of magnesium in determining the bioactivity of glasses is yet to be studied in detail [22]. However, several attempts have been made to explore the role of magnesium and its ability to form an apatite layer. Different opinions have been expressed on the effect of the addition of MgO content to glass network [23–27]. An attempt has been made to develop a glass with high MgO content (17.25 wt%) and to show the formation of a Ca–P-rich layer after immersion in a simulated body fluid (SBF) solution [28]. The phosphate-containing biocompatible glasses have received more attention as implantable material because of

* Corresponding author. Tel.: +91 4288 274741–4; fax: +91 4288 274880.
E-mail address: veerajendraan@gmail.com (V. Rajendran).

0272-8842/$36.00
doi:10.1016/j.ceramint.2012.01.026

their flexibility in controlling the solubility of glasses [29]. Phosphate glasses have been considered as potential candidates for repair and reconstruction of bone. The structure of phosphate glass, namely PO_4 tetrahedra with a three-dimensional network, is similar to that of vitreous P_2O_5.

The addition of metal oxide leads to the depolymerisation of network with oxygen atoms breaking the P–O–P links and creating NBOs in glass network [7,11,19]. The structure of polyphosphate glasses is based on Q^2 chains terminated by Q^1 units. (In Q^n terminology, n represents the number of bridging oxygens per PO_4 tetrahedra.) The addition of network-modifying oxides leads to the depolymerisation of phosphate chains. When 0.5 mol% of metal oxide is added to metaphosphate glasses, it gives out infinite long-chain Q^2 units. Ultrasonic studies have been widely accepted as a promising tool for exploring the mechanical properties of glasses [30,31]. This is possible because of the interactions of ultrasonic waves with macro-, micro- and submicroscopic particles during the propagation of ultrasonic waves into glass, and because of the availability of multimode vibrations and a wide range of frequencies to select from.

In this investigation, an attempt has been made to study the role of MgO in the physico-chemical properties and HAp-forming ability of prepared glass samples. Five different compositions of phosphate-based glass samples were prepared by keeping a constant ratio of P/Ca (=3.0) with the addition of MgO in place of Na_2O. Methods such as X-ray diffraction (XRD), differential thermal analysis (DTA), energy-dispersive X-ray spectroscopy (EDS), pH, Fourier transform infrared spectroscopy (FTIR), scanning electron microscopy (SEM) and ultrasonic velocities were used widely to study the structure, glass transition temperature (T_g), chemical composition, solubility, functional groups/structural changes, surface morphology and mechanical properties of the prepared glasses, respectively.

2. Experimental procedure

2.1. Preparation of glass samples

The $45P_2O_5$–30CaO–$(25 - x)Na_2O$–xMgO glass of different compositions ($x = 0$, 1, 2.5, 5 and 10 mol%) was prepared using commercially available chemicals by the normal melting quench method [11]. Glasses with different MgO contents, $x = 0$, 1, 2.5, 5 and 10 mol% (hereafter termed as PCNM0, PCNM0.25, PCNM0.5, PCNM0.75 and PCNM1.0, respectively), were prepared. The chemical components included $NH_4H_2PO_4{\cdot}2H_2O$ (99.999%), $CaCO_3$ (99.995%), Na_2CO_3 (99.9%) and MgO (99%), which were of analytical grade (Sigma–Aldrich, Bangalore, India) and used without any further purification. The aim of this study was to evaluate how the addition of MgO influences network modification, hydroxyapatite (HAp) nucleation and bioactivity [32]. The exact weight of each chemical reagent was measured using a digital balance (model BP221S; Sartorius, Goetttingen, Germany) and ground using a ball mill (model PM 100; Retch, Haan, Germany) with agate balls of 10-mm diameter. The mixture was melted in an alumina crucible for 3 h at 1300 K in an electric furnace.

The homogenized melt was recast in a preheated graphite mould of rectangular shape with a size of 90 mm × 60 mm × 20 mm. The prepared glass sample was annealed at 573 K for 1 h in an electric furnace. Further, the glass sample was cooled to room temperature at a rate of 1 K min^{-1}. Five discs (12-mm diameter and 6-mm thickness) and six rectangular glass samples (12 mm × 12 mm × 6 mm) were cut from the prepared glasses using a diamond saw for *in vitro* studies and for ultrasonic velocity measurements, respectively. The plane parallelism between the surfaces of glass samples was checked using a surface plate and a dial gauge. The glasses were shaped in the form of discs of 10-mm diameter with 6–7-mm thickness. The samples were initially rinsed with acetone, and again with ethanol to remove any foreign particle residues. The percentage error in measurement of glass thickness was ±0.01.

2.2. Characterization

2.2.1. Density measurements

The density of prepared glass samples was obtained using Archimedes' principle with CCl_4 as a buoyant. The density of glass was calculated using a standard equation ($\rho = W_a/[W_aW_b] \times \rho_b$), where W_a is the weight in air, W_b the weight in buoyant and ρ_b the density of the buoyant. All weight measurements were taken using a digital balance having an accuracy of $\pm 0.0001 \times g$. The experiment was repeated five times to obtain an accurate value of density. The overall accuracy of density measurement was ±0.5 kg m^{-3}. The percentage error in measurement of density was ±0.05.

2.2.2. Ultrasonic measurements

Longitudinal and shear ultrasonic velocity measurements were taken in each glass using a cross-correlation technique by adopting pulse echo method [30]. The ultrasonic process control system (model FUII050; Fallon Ultrasonics Inc. Ltd., Ontario, Canada), with a 100 MHz digital storage oscilloscope (model 54600B; Hewlett Packard, Palo Alto, CA, USA), and a computer were used for recording ultrasonic (rf) signals. X- and Y-cut transducers that operated at a fundamental frequency of 5 MHz were used for both generation and detection of longitudinal and shear waves, respectively. The ultrasonic velocity (U_L and U_S) in glass was calculated using the standard equation $U = 2 \times d/t$, where d is the thickness of the glass and t the precise transit time [30]. The percentage error in the measurement of velocity was ±1.

The attenuation coefficient (α_L/α_S) was calculated by measuring peak amplitude of the successive back wall echo signal from glass samples using the equation $\alpha = [-20/\{2 \times (m - n) \times d\}] \times \log[I_m/I_n]$, where I_m and I_n are the maximum amplitude of the mth and nth pulse echo in voltage, respectively. The percentage error in attenuation measurement was ±2 [30]. The precise ultrasonic velocity and attenuation measurements were taken using the procedure discussed elsewhere [30]. A suitable couplant (honey) was used to

obtain a steady back wall echo train and the necessary couplant correction for velocity and attenuation was carried out as discussed earlier [31].

2.2.3. Elastic constants

Elastic moduli such as longitudinal (L), shear (G), bulk (K), Young's (E) and Poisson's ratio (σ) and microhardness (H) were obtained from the experimental values of density (ρ), longitudinal velocity (U_L) and shear velocity (U_S) as described elsewhere [19]. Using the above relations, the elastic moduli, microhardness and Poisson's ratio of each glass sample were calculated from ultrasonic velocity measurement and its density value. The percentage of error in measurement of moduli was ± 2.

2.2.4. X-ray diffraction analysis

X-ray diffraction studies were carried out on each glass sample to confirm the amorphous nature of prepared glasses and the existence of HAp layer on the surface of glass samples before and after *in vitro* studies respectively. An X-ray diffractometer (PW 1700; Philips, Eindhoven, The Netherlands) was used with CuK_α as a radiation source for obtaining the XRD pattern in the range of a scanning angle between 20° and 80° [19].

The prepared glass sample and the sample that was removed from SBF solution after *in vitro* studies were washed gently in double-distilled water. The washed glass sample was dried at room temperature, ground and then used to obtain the XRD pattern as discussed above. This procedure will help to understand the nature of glass and the formation of HAp layer on the given sample before and after 21 days *in vitro* studies.

2.2.5. Energy dispersive X-ray spectroscopy analysis

Energy dispersive X-ray spectroscopy (model JED-2300; JEOL, Tokyo, Japan) was used to determine the experimental composition of prepared glass samples. EDS studies helped to explore the loss of raw material during grinding and melting processes in the samples.

2.2.6. Differential thermal analysis

Differential thermal analysis was carried out using a Thermal Analyser (PerkinElmer Diamond, Waltham, MA, USA) at a heating rate of 10 K min^{-1} under a stream of high-purity nitrogen atmosphere. The glass transition temperature (T_g) for each glass was obtained from corresponding DTA curve using the general procedure used for the determination of T_g, *i.e.*, the crossing point of the two straight lines, as discussed elsewhere [33]. The measurement was carried out five times and the average T_g value was taken in order to minimize the error in T_g measurement. The error in the measurement of T_g obtained was less than ± 1 K.

2.2.7. In vitro studies

The HAp-forming ability of prepared glasses was carried out by 21 days of *in vitro* studies in SBF solution. The SBF solution was prepared using the standard procedure formulated by

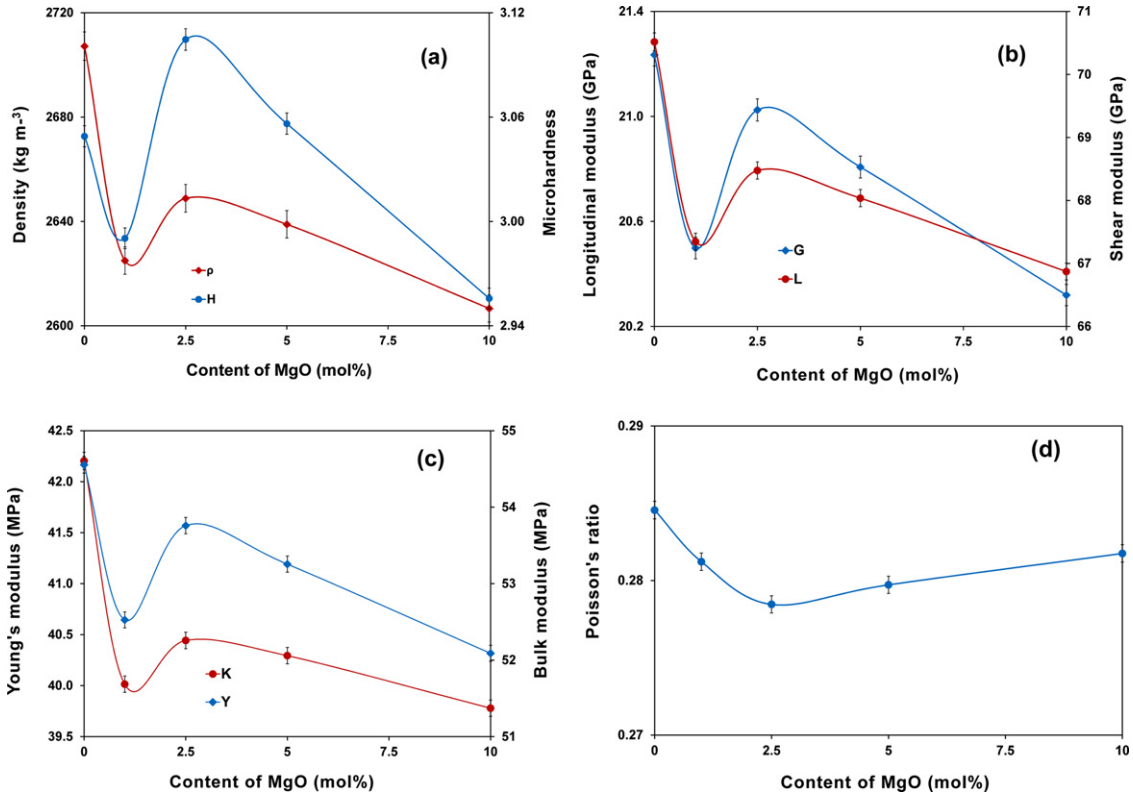

Fig. 1. Acoustical parameter as a function of MgO content. Error bars represent ± 1 standard deviation. (a) Variation of density and microhardness with change in MgO content. (b) Variation of longitudinal (L) and shear modulus (G) with MgO content. (c) Variation of Young's (Y) and bulk (K) modulus with MgO content. (d) Variation of Poisson's ratio (σ) with MgO content.

Table 1
Ultrasonic longitudinal velocity (U_L), shear velocity (U_S), longitudinal attenuation (α_L), shear attenuation (α_S), and density (ρ), glass transition temperature (T_g) along with the composition of phosphate based glass at 303 K.

Sample code	Glass composition (mol%)				Density (kg m^{-3})	T_g (K)	Velocity (m s^{-1})		Attenuation (dB cm^{-1})	
	P_2O_5	CaO	Na_2O	MgO	ρ		U_L	U_S	α_L	α_S
PCNM0	45 (66.40)[a]	30 (17.49)[a]	25.0 (16.11)[a]	0 (0)[a]	2707 ± 3	648 ± 1	5104 ± 5	2801 ± 3	0.08	0.06
PCNM1	45 (66.23)[a]	30 (17.45)[a]	24 (15.91)[a]	1 (0.42)[a]	2625 ± 4	642 ± 1	5065 ± 5	2795 ± 4	0.08	0.06
PCNM2.5	45 (66.78)[a]	30 (17.59)[a]	22.5 (14.58)[a]	2.5 (1.05)[a]	2649 ± 1	645 ± 1	5084 ± 4	2817 ± 3	0.07	0.06
PCNM5	45 (67.16)[a]	30 (17.69)[a]	20 (13.03)[a]	5 (2.12)[a]	2639 ± 3	642 ± 1	5078 ± 5	2808 ± 2	0.08	0.06
PCNM10	45 (67.93)[a]	30 (17.89)[a]	15 (9.89)[a]	10 (4.29)[a]	2607 ± 1	640 ± 1	5065 ± 3	2792 ± 3	0.08	0.06

[a] The compositions in wt.% is inside the bracket.

Kokubo et al. [34,35]. The pH value of the prepared SBF solution was equivalent to the pH value of human blood plasma. Analytical-grade chemicals (99.95%; Sigma–Aldrich) were added suitably while stirring continuously in a polyethylene container to prepare SBF solution. The prepared SBF solution was kept at 278 K for 48 h to explore the presence of any precipitates. The prepared solution was suitable for *in vitro* studies only if there was no precipitation. Each glass sample was immersed in SBF solution for 21 days under identical conditions at 310 K in a polyethylene container. After 21 days of soaking, the glass samples were taken out from SBF solution and washed with distilled water, followed by drying at room temperature. The results from XRD, FTIR and SEM studies on the glass samples before and after soaking in SBF solutions were obtained and used to explore the structural changes and HAp-forming ability.

2.2.8. *pH measurements*

Variation in the pH values of SBF solutions was measured every day in all glasses under identical conditions during 21 days of *in vitro* studies using a pH meter (Model 720A; Thermo Orion, Beverly, MA, USA). The pH electrode was calibrated using the standard pH values of 4.01, 7.00 and 10.01 before taking pH measurements. The percentage error in the measurement of pH was ±0.005.

2.2.9. *Scanning electron microscopy*

The glass samples were gently washed with double-distilled water and dried at room temperature. A thin layer of gold film was coated on the surface of glass samples using a sputtering technique. The scanning electron microscope (model 514A; Hitachi, Tokyo, Japan) was used to explore the surface morphology of all glass samples. A micrograph was used to confirm the formation of Ca–P layers on the surface of glasses after *in vitro* studies.

2.2.10. *Fourier transform infrared analysis*

The infrared absorption of powdered glass samples was analysed from FTIR patterns. FTIR absorption spectra were recorded at room temperature from 4000 to 400 cm^{-1} using an FTIR (model 8700; Shimatzu, Tokyo, Japan) spectrometer. Samples of 2.0 mg each was mixed with 200 mg of KBr in an agate mortar and then pressed to a pressure of 100 kg cm^{-2} and a pellet of 13-mm diameter was obtained [19]. For each sample, the FTIR spectrum was normalized with a blank KBr pellet. The pellet was prepared by mixing about 2 mg of materials scrapped from glass surface with KBr. These studies were carried out in all glass compositions before and after *in vitro* studies.

3. Results

The observed density, T_g value, ultrasonic velocities (U_L and U_S) and attenuation (α_L and α_S) of prepared glass samples for different MgO contents are given in Table 1. A sudden decrease in density and ultrasonic velocities (U_L and U_S) is observed when 1 mol% of MgO was added to base glass PCNM0. The composition-dependent properties show a small increase in

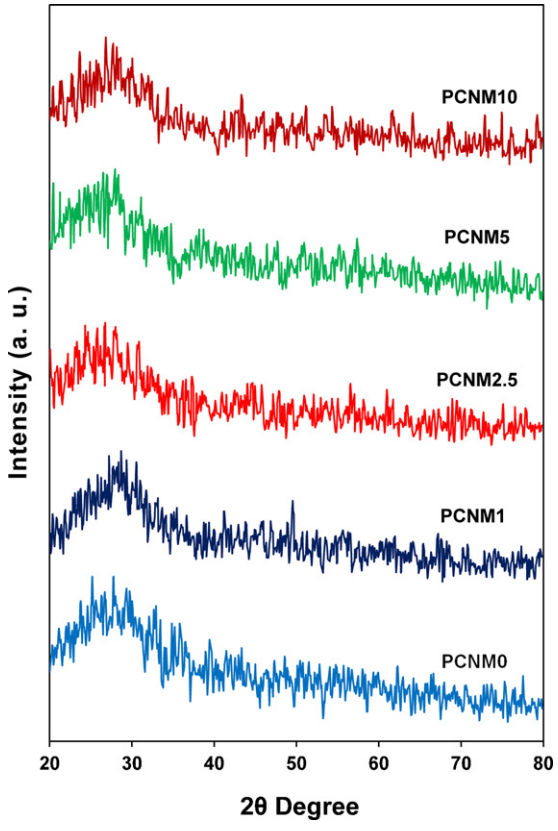

Fig. 2. XRD patterns of bioactive glass samples before immersed in SBF.

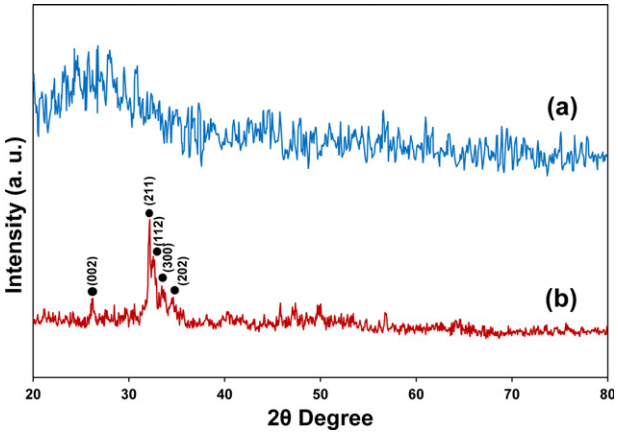

Fig. 3. XRD patterns of bioactive glass sample PCNM2.5. (a) before and (b) after *in vitro* studies.

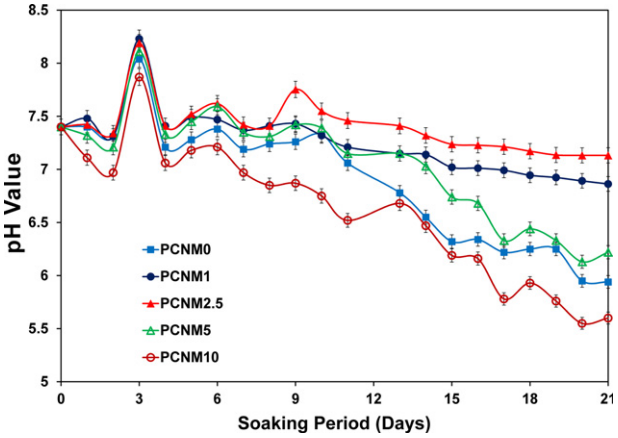

Fig. 4. pH value as a function of soaking period of SBF solutions.

density and ultrasonic velocities after the addition of MgO content up to 2.5 mol%, beyond which a gradual decrease in density and velocities is observed with the further addition of MgO content as shown in Fig. 1a.

The variation in mechanical properties, such as microhardness (H), longitudinal (L) and shear (G), Young's (Y) and bulk (K) moduli and Poisson's ratio is shown in Fig. 1a–d. The elastic moduli and microhardness reveal a trend similar to that of density and velocities. However, Poisson's ratio (σ) remains almost constant with a small change from 0.279 to 0.285 due to the change in MgO content from 0 to 10 mol% as observed in Fig. 1d. The attenuation (α_L and α_S) shows a trend opposite to that of density and velocities in all compositions.

The observed XRD patterns before *in vitro* studies in all glasses are shown in Fig. 2, which confirms their amorphous nature. The XRD patterns that are observed on PCNM2.5 glass sample, before and after *in vitro* studies, are shown in Fig. 3 for comparison. The obtained peaks, such as 26.150°, 31.8829°, 32.214°, 32.770° and 34.596°, correspond to crystal planes (0 0 2), (2 1 1), (1 1 2), (3 0 0) and (2 0 2) of HAp. The above-mentioned results confirm the presence of HAp and the precipitation of Ca–P layer on the surface of the glasses.

The obtained experimental composition of all the prepared glasses from EDS studies is given in Table 2. The corresponding mol% of experimental composition of each glass is given within brackets for comparison. There were no traces of alumina residue in the prepared glass samples. The differences between the experimental and nominal composition of glasses are within ±2%. The T_g value is obtained for all glass samples

Table 2
Experimental and nominal composition of the glasses investigated.

Sample code	P_2O_5 (mol%)	CaO (mol%)	Na_2O (mol%)	MgO (mol%)
PCNM0	45 (45.83)[a]	30 (29.42)[a]	25.0 (24.57)[a]	0 (0)[a]
PCNM1	45 (45.89)[a]	30 (29.50)[a]	24 (23.59)[a]	1 (1.02)[a]
PCNM2.5	45 (45.87)[a]	30 (29.51)[a]	22.5 (22.11)[a]	2.5 (2.51)[a]
PCNM5	45 (45.84)[a]	30 (29.52)[a]	20 (19.74)[a]	5 (4.90)[a]
PCNM10	45 (45.91)[a]	30 (29.51)[a]	15 (14.74)[a]	10 (9.84)[a]

[a]The nominal composition is inside the bracket.

from DTA studies (Figures not given). The composition-dependent T_g value is shown in Table 1. An initial decrease in T_g value is observed up to the addition of 1.0 mol% of MgO content on the base glass. The same increases with further addition of MgO up to 2.5 mol%. Beyond the addition of 2.5 mol% of MgO content, a decrease in T_g value is noted. The change in T_g value in the present glass system indicates three distinct types of behaviour in glass network as a function of MgO content.

The scanning electron micrographs of prepared glass samples such as PCNM2.5 before *in vitro* studies along with PCNM0, PCNM1, PCNM2.5, PCNM5 and PCNM10 after 21 days of immersion in SBF solution are shown in Fig. 5a–f. These figures show changes that occurred in the morphology of soaked glass surface as a function of MgO content. It is evident that the base glass (PCNM0) forms a thin porous precipitate layer, namely, HAp. The amount of formation of porous precipitation increases with increase in MgO from PCM0 to PCNM1 and from PCNM1 to PCNM2.5. However, the amount

Table 3
The predominant variations in pH values.

Sample code	pH variations			Nature of the SBF solution on 21st day	Bioactivity level
	Day 0	Day 3	Day 21		
PCNM0	7.4	8.041 ± 0.001	5.941 ± 0.002	Acid	Low
PCNM1	7.4	8.234 ± 0.002	6.863 ± 0.002	Weak acid	High
PCNM2.5	7.4	8.192 ± 0.001	7.132 ± 0.001	Neutral	High
PCNM5	7.4	8.114 ± 0.001	6.131 ± 0.001	Acid	Medium
PCNM10	7.4	7.874 ± 0.001	5.550 ± 0.002	Acid	Nil

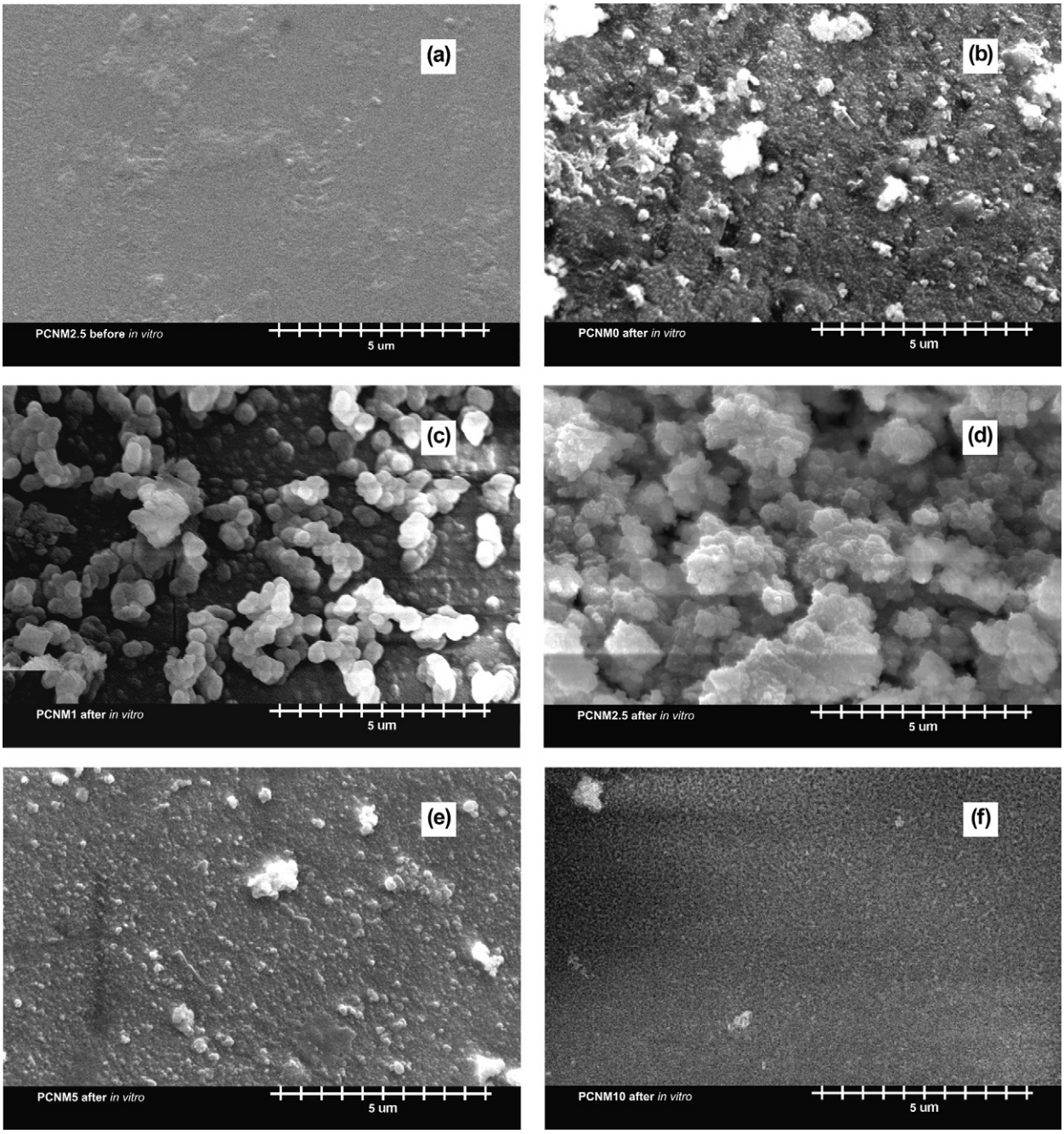

Fig. 5. SEM micrograph of the surface of the sample before *in vitro* studies (a) PCNM2.5, after *in vitro* studies, (b) PCNM0, (c) PCNM1, (d) PCNM2.5, (e) PCNM5 and (f) PCNM10.

of formation of HAp layer on glass surface after 21 days of *in vitro* studies in PCNM5 is found to be less when compared with PCNM0, PCNM1 and PCNM2.5 glass surfaces. However, PCNM10 does not reveal the formation of HAp on the glass surface after *in vitro* studies.

The change in pH value of SBF solution with time in all glass samples is shown in Fig. 4. The predominant variations in pH value during 21 days of *in vitro* studies are shown in Table 3. The obtained results suggest the influence of MgO content on base glass PCNM0. It is evident that there is a significant increase in pH value of the prepared SBF solution up to 8.2, beyond which there is a slow decline and it ends with different pH values (Fig. 4). The pH value of SBF solution, which contains PCNM1 and PCNM2.5 glasses, shows a gradual variation and it reaches the neutral pH value (∼7) at the end of 21 days of *in vitro* studies. The pH values of remaining samples, PCNM0, PCNM5 and PCNM10, show a random decrease towards acidic nature.

Figs. 6 and 7 show FTIR analysis of all prepared glass samples (PCNM0, PCNM1, PCNM2.5, PCNM5 and PCNM10) before and after 21 days of immersion in SBF solution. The observed prominent characteristic absorption bands and corresponding modes are shown in Table 4. In the spectrum

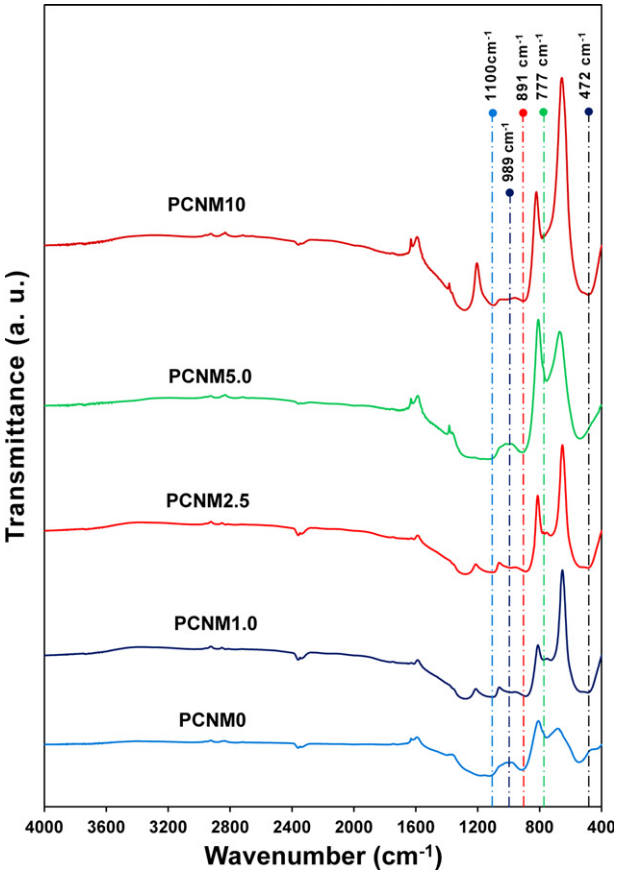

Fig. 6. FTIR transmittance spectra of bioactive glass samples before immersion in SBF solution.

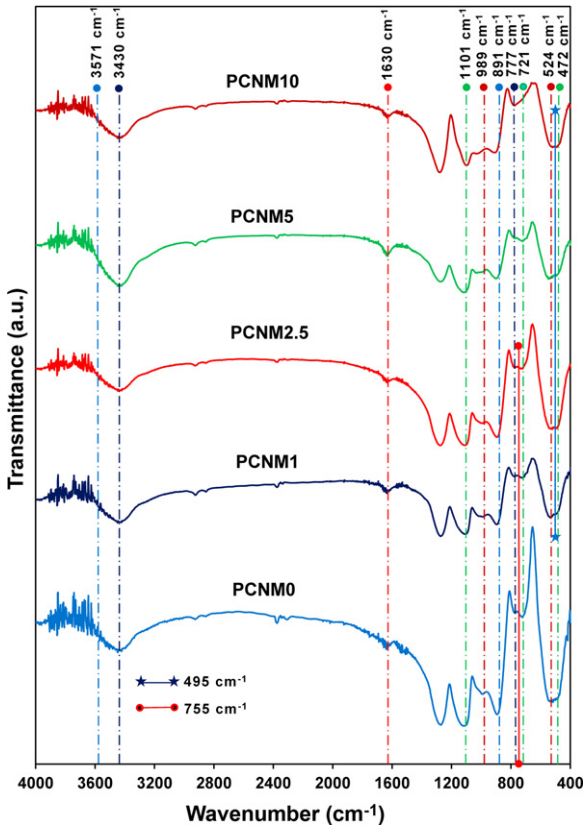

Fig. 7. FTIR transmittance spectra of bioactive glass samples after 21 days of immersion in SBF solution.

of samples before and after *in vitro* studies, one can observe an absorption peak at 472 cm^{-1} corresponding to O–P–O bending mode of PO_4^{3-} [36]. The observed absorption frequencies at 777, 891, 989 and 1100 cm^{-1} correspond to stretching mode of symmetric P–O–P, P–O and PO_3 bonds and to asymmetric mode of PO_3 bonds, respectively [27,36,37]. Interestingly, after *in vitro* studies, a characteristic absorption due to symmetric bending mode of β-$Ca_2P_2O_7$ at 495 cm^{-1} was obtained only after doping of MgO (PCNM1, PCNM2.5, PCNM5 and PCNM10). In other words, this characteristic absorption is not presented in base glass PCNM0. An asymmetric bending mode of PO_3 is recorded at 525 cm^{-1} [37]. After the *in vitro* studies, we found absorption at 755 cm^{-1} corresponding to P–O–P stretching vibrations of α-$Ca_2P_2O_7$, in glasses PCNM0, PCNM1 and PCNM2.5 [37]. The same absorption band was shifted towards the high-frequency side in glass samples PCNM5 and PCNM10. The absorption peak at 721 cm^{-1} indicates the existence of P–O–P stretching mode of vibration

Table 4
FTIR absorption bands of MgO added glass system.

Wave numbers (cm^{-1})										Assignments	Ref.
Before *in vitro*					After *in vitro*						
PCNM0	PCNM1	PCNM2.5	PCNM5	PCNM10	PCNM0	PCNM1	PCNM2.5	PCNM5	PCNM10		
472	472	472	472	472	474	472	471	472	474	O–P–O bending mode of PO_4^{3-}	[36]
–	–	–	–	–	–	495	495	495	495	Absorption band of β-$Ca_2P_2O_7$	[36]
–	–	–	–	–	525	524	524	520	521	δ_{as} PO_3 asymmetric mode	[37]
–	–	–	–	–	721	721	721	721	721	v_s P–O–P stretching mode	[37]
					755	755	755	–	–	P–O–P vibrations of α-$Ca_2P_2O_7$	[37]
777	777	777	777	777	777	777	777	777	777	Symmetric stretching of P–O–P	[37]
891	891	891	891	891	895	895	895	895	895	P–O stretching mode	[36]
989	989	989	989	989	989	989	989	989	989	PO_3 stretching mode	[27]
1100	1103	1101	1103	1100	1110	1106	1103	1103	1100	v_{as} PO_3 asymmetric mode	[37]
–	–	–	–	–	1630	1630	1630	1630	1630	Bending mode of HCO_3	[38]
–	–	–	–	–	3430	3430	3430	3430	3430	OH stretching mode of water	[38]
–	–	–	–	–	–	3571	3571	3571	–	OH stretching vibration	[41]

after *in vitro* studies [37]. Similarly, the observed absorption band at 3430 and 1630 cm^{-1} in all samples are attributed respectively to stretching mode of O–H group and bending mode of HCO_3^- [38–40]. The stretching mode vibration of OH group was recorded exclusively at 3571 cm^{-1} for glass samples PCNM1, PCNM2.5 and PCNM5 [41].

4. Discussion

The density of glass samples has been used as a tool to explore its structural changes and cross-link density [42]. The addition of network modifiers disrupts the bonds and thus lowers crosslink density, leading to an increase in the number of NBO atoms present in the glass system [43]. The initial addition of MgO to the base glass results in an increase in NBO networks, such as Q^1 and Q^2 of PO_4 tetrahedra. As a result, a decrease in density takes place on glass sample PCNM1. In other words, an initial addition of network modifier, namely MgO, leads to breaking of P–O–P bonds in phosphate network and results in the formation of terminal oxygens. A further addition of MgO up to 2.5 mol% reveals the incorporation of Mg^{2+} ions into interstitial positions in glass network through NBOs. This results in an increase in packing density, followed by structural compactness, which leads to an increase in density of glass sample PCNM2.5. It is interesting to note that when MgO is added beyond 2.5 mol%, a break in the network structure results in the isolation of PO_4 tetrahedra. Hence, loose packing of atoms leads to structural softening. The observed microhardness reveals a trend similar to that of density. An increase in the structural softening of glass network up to a maximum of 20 wt% of LiO_2 in the binary silicate glass system was observed [44]. A further addition of alkali oxides beyond 20 wt% leads to breakage of the network structure because of the formation of more NBOs. The above-mentioned study of structural changes in binary silicate glass added to the alkali material supports the present observation.

In this study, the P/Ca ratio of all prepared samples was kept constant at 3.0. The composition dependence of velocities shows a trend similar to that of density. The initial decrease in velocities (both U_L and U_S) and an increase in attenuation are observed when 1 mol% of MgO is added to base glass sample PCNM0. The longitudinal, Young's, shear and bulk moduli show a trend similar to that of velocities. The change in the behaviour of velocities and attenuation beyond 2.5 mol% of MgO content is similar in nature to that of density. This may be because of the incorporation of a smaller ionic radius and a large charge in MgO into the glass network through NBOs. Thus, structural compactness takes place and an increase in density and velocities and a decrease in attenuation were noticed. The observed change in velocities and elastic moduli beyond 2.5% of MgO reveals a decreasing trend due to loose packing of atoms, that is, structural softness [8].

The structure of glasses is correlated with the thermal stability of the glass network [19]. A closely packed structure leads to thermally stable glasses, whereas a loosely packed structure leads to unstable glasses. In the present study, a decrease in glass transition temperature (T_g) from 648 to 640 K with the addition of MgO content up to 1.0 mol% is noticed. The same is increased with the addition of MgO content up to 2.5 mol%. A decrease in T_g value beyond 2.5 mol% of MgO content is also noticed. Even though the glass transition temperature explores the structural changes taking place in the glass network, the addition of MgO to the base glass results in small changes in the T_g value in the present study.

A close agreement between experimental and nominal composition is noticed from EDS analysis (Table 2). Further, no evidence for impurities such as silica, alumina, etc. is obtained in the glass samples. The XRD patterns obtained before *in vitro* studies confirm the amorphous nature of glasses (Fig. 2). The XRD patterns (PCNM2.5) obtained after *in vitro* studies confirm the presence of HAp, which is evident from the observed peak at diffracted angles (2θ) 26.150, 31.8829, 32.214, 32.770 and 34.596°, which corresponds to crystal planes (0 0 2), (2 1 1), (1 1 2), (3 0 0) and (2 0 2), respectively (JCPDS 09-0432 $Ca_{10}(PO_4)_6(OH)_2$) [11].

The rate of biodegradation of bioactive material is complex and has an important role and significantly affects its stability after implant. The study of the soluble nature of prepared glass samples during *in vitro* study is considerably helpful for optimisation. The ions in the SBF solution, such as Cl^-, HCO_3^- and HPO_4^{2-}, affect glass network by exchanging PO_4^{3-}, Ca^{2+} and Na^+ ions from the glass sample, which is available in SBF solution.

The increase in pH value of SBF solution due to release of Na^+ accelerates the formation of apatite layer as reported elsewhere [3]. The later decrease in pH value with an increase in time is mainly due to the increase in the solubility of glasses and due to decrease in Na^+ ion content [3]. During *in vitro* studies, the immediate release of Na^+ from glass samples may lead to an increase in the pH value of the SBF solution (initial pH value is 7.4) up to 8.23. Thus, it is possible to make a sudden change in the pH value of the SBF solution in all glass samples within 3 days of immersion. The increase in the dissolution rate of glasses leads to a decrease in the pH value of the solution. The change in pH value ensures the exchange of ion between glass and the SBF solution. A similar behaviour of the pH value was observed in different phosphate-based glasses after immersion in an SBF solution [11,19,24,45]. The exchange of ions during *in vitro* studies is one of the essential reactions to ensure the formation of the HAp layer. After the third day, the phosphate ion started to release and dominate the Na^+ concentrations. Thus, a decreasing trend in the pH value is observed after the third day. The observed linear and non-linear variations in the pH value of the SBF solution were extensively studied for P_2O_5–CaO–Na_2O glass systems by Franks et al. [46]. The above-mentioned studies support our observations, that is, of the observed high initial pH value followed by a non-linear variation with change in time (Fig. 4). P_2O_5 is a network-forming component and hence the dissolved phosphate is directly linked to the dissolution of the glass sample. The solubility of glass strongly depends on its composition.

It is evident from the results mentioned above that the glass sample PCNM2.5 has a compact structural glass network, as described by the density measurements. An increase in

solubility of glasses due to addition of metal oxide and, hence the structural compactness, has been widely shown [11]. As a result, the controlled dissolution leads to a reduction in the release of PO_4^{3-} ions and thus results in less variation in pH value after the third day. The density of glass samples PCNM5 and PCNM10 is low when compared with the PCNM2.5 sample, which is due to the observed loose packing of the glass network [8]. Filgueiras et al. have discussed the role of magnesium ions, which are not significantly affected by SBF compositions; however, the solubility of the glass sample has been found to increase with addition of MgO content [47]. This phenomenon increases the solubility of the glass sample and releases PO_4^{3-} ions. These PO_4^{3-} ions increase its acidity and hence a decrease in the pH value of SBF solution is obtained, which contains glass samples PCNM5 and PCNM10.

The differences among the five SEM micrographs show the influence of MgO content in the formation of HAp layer on glass surface. The SEM micrograph of sample PCNM2.5 before *in vitro* studies (Fig. 5a) shows no precipitate or layer on its surface. After *in vitro* studies, the sample without the addition of MgO shows a low growth of Ca–P layer (Fig. 5b), whereas the glass PCNM10 does not show any trace of growth of a new layer on the surface; rather, it shows a dry surface (Fig. 5f). The SEM micrographs of the remaining three glasses, namely PCNM1, PCNM2.5 and PCNM5 (Fig. 5c–e), confirm the increase in the rate of growth of Ca–P layer with an increase in MgO content. From the SEM micrographs that are observed the rate of formation of Ca–P layer is highly pronounced in glass sample PCNM2.5 compared with other glasses. Kasuka et al. have investigated the role of MgO in glasses and glass ceramics in $CaO–P_2O_5–SiO_2–MgO$ glass systems [25]. It has been found that the ability to form an apatite layer on glass ceramics decreases with an increase in MgO content. As a result, glass ceramics with more than 8 wt% of MgO do not show the formation of the HAp layer. SEM studies (Fig. 5d) confirm the formation of a higher amount of HAp layer on sample PCNM2.5 in which the glass sample PCNM10 does not show the formation of HAp.

In general, Q^0, Q^1 and Q^2 phosphate absorption bands are found between 1400 and 400 cm^{-1} [48]. The observed FTIR spectra indicate the presence of Q^0, Q^1 and Q^2 species at 891, 989 and 1103 cm^{-1} in all glass samples, respectively. The higher intensity of band observed at 891 cm^{-1} shows the greater concentration of Q^0. The intensity of the above peak at 891 cm^{-1} decreases as MgO content increases. These results support the finding that the density of PO bonds decreases with the addition of MgO. It has been noted that the role of Mg^{2+} in the formation of a Ca–P-rich layer was observed as being insignificant [27]. However, the MgO content in glass samples leads to an increase in the dissolution rate of magnesium.

In this study, all samples before and after *in vitro* studies show a broad band at 1103, 989 and 895 cm^{-1}, which corresponds to the stretching mode of symmetric PO_3, P–O and P–O–P bonds, respectively. Similarly, the observed absorption bands at 721 and 777 cm^{-1} show the asymmetric mode of vibration of PO_3 bond. The observed peaks at 472 cm^{-1} show the presence of phosphate vibrations in all glass samples. The absorption band that is observed at 755 cm^{-1} is noted in samples PCNMO, PCNM1 and PCNM2.5 after *in vitro* studies, which is evidence of the P–O–P vibration of α-$Ca_2P_2O_7$. The above-mentioned absorption band is shifted towards a higher frequency side for PCNM5. This characteristic band does not appear in PCNM10. The above-mentioned results confirm that a considerable amount of calcium phosphate is present in samples PCNM0, PCNM1, PCNM2.5 and PCNM5, whereas there is no evidence of the presence of this layer in sample PCNM10.

Similarly, the absorption frequency observed at 495 cm^{-1} shows the presence of β-$Ca_2P_2O_7$ in all glass samples except in the base glass PCNM0. This result supports the finding that the addition of MgO content initiates the formation of the β-$Ca_2P_2O_7$ layer. Further, the observed absorption band at 1630 cm^{-1} confirms the presence of $CaHPO_4{\cdot}2H_2O$ in all glass samples [40]. The absorption band at 3571 cm^{-1} indicates the OH stretching vibrations, which are absent in samples PCNM0 and PCNM10. Thus, the above studies confirm the presence of OH vibrations in low MgO content, *i.e.*, below 5 mol%, beyond OH vibrations are not present.

5. Conclusions

In this investigation, $P_2O_5–CaO–Na_2O$ glass samples with different MgO (replacing Na_2O) contents by keeping the P/Ca ratio as 3.0 are prepared and characterised by density, ultrasonic, pH, XRD, FTIR and SEM studies. The observed minimum in density, velocities and modulus and the maximum in attenuation with change in MgO content up to 1 mol% indicate the softening of the glass network. The addition of MgO content up to 2.5 mol% increases the structural compactness of glass network. Further, the addition of MgO beyond 2.5 mol% resulted in a loose packing of atoms, leading to structural softening. The ultrasonic velocities and attenuation measurements show the same trend as that of density. After the third day of *in vitro* studies, the phosphate ion starts to release and dominate acidity because of phosphate molecules. Therefore, a random change from the third day onwards is noticed. The FTIR studies confirmed the presence of a CaP layer in all prepared samples. The observed absorption bands in all glasses after *in vitro* studies at 3430 and 1630 cm^{-1} confirm the presence of OH groups and calcium apatite crystal, respectively. These results confirmed the existence of OH vibrations in glass samples with the addition of low MgO content, *i.e.*, below 5 mol%, beyond which OH vibrations are not present. However, the SEM studies show the formation of a strong and porous precipitate layer in sample PCNM2.5 compared with other samples. The XRD results on sample PCNM2.5 after *in vitro* studies confirm the presence of HAp on its surface. It is inferred from these results that the PCNM2.5 glass sample exhibits higher HAp-forming ability compared with other glass samples.

References

[1] S. Fujibayashi, M. Neo, H.-M. Kim, T. Kokubo, T. Nakamura, A comparative study between in vivo bone ingrowth and *in vitro* apatite formation on $Na_2O–CaO–SiO_2$ glasses, Biomaterials 24 (2003) 1349–1356.

[2] W. Lai, J. Garino, P. Ducheyne, Silicon excretion from bioactive glass implanted in rabbit bone, Biomaterials 23 (2002) 213–217.

[3] I. Ahmed, M. Lewis, I. Olsen, J.C. Knowles, Phosphate glasses for tissue engineering: Part 1. Processing and characterisation of a ternary-based P_2O_5–CaO–Na_2O glass system, Biomaterials 25 (2004) 491–499.

[4] J. Burnie, T. Gilchrist, S.R.I. Duff, C.F. Drake, N.G.L. Harding, A.J. Malcolm, Controlled release glasses (C.R.G.) for biomedical uses, Biomaterials 2 (1981) 244–246.

[5] T. Kasuga, Y. Hosai, M. Nogami, Apatite formation on calcium phosphate invert glasses in simulated body fluid, J. Am. Ceram. Soc. 84 (2001) 450–452.

[6] K. Franks, I. Abrahams, G. Georgiou, J.C. Knowles, Investigation of thermal parameters and crytallisation in a ternary CaO–Na_2O–P_2O_5-based glass system, Biomaterials 22 (2001) 497–501.

[7] V. Rajendran, A.V. Gayathri Devi, M. Azooz, F.H. El-Batal, Physico-chemical studies of phosphate based P_2O_5–Na_2O–CaO–TiO_2 glasses for biomedical applications, J. Non-Cryst. Solids 353 (2007) 77–84.

[8] G. Rajkumar, M. Rajkumar, V. Rajendran, S. Aravindan, Influence of Ag_2O in physico-chemical properties and HAp precipitation on phosphate-based glasses, J. Am. Ceram. Soc. 94 (2011) 2918–2925.

[9] J.M. Oliveira, R.N. Correia, M.H. Fernandes, Surface modifications of a glass and a glass-ceramic of the MgO–3CaO–P_2O_5–SiO_2 system in a simulated body fluid, Biomaterials 16 (1995) 849–854.

[10] Manupriya, K.S. Thind, G. Sharma, V. Rajendran, K. Singh, A.V. Gayathri Devi, S. Aravindan, Structural and acoustic investigations of calcium borate glasses, Phys. Status Solidi (a) 203 (2006) 2356–2364.

[11] V. Rajendran, G. Rajkumar, S. Aravindan, Analysis of physical properties and hydroxyapatite precipitation in vitro of TiO_2-containing phosphate-based glass systems, J. Am. Ceram. Soc. 93 (2010) 4053–4060.

[12] L.L. Hench, Bioceramics: from concept to clinic, J. Am. Ceram. Soc. 74 (1991) 1487–1510.

[13] W. Vogel, W. Holand, Development of glass–ceramics for medical application, Angew. Chem. Int. Ed. Engl. 26 (1987) 527–544.

[14] W. Vogel, W. Holand, Development, structure, properties and application of glass–ceramics for medicine, J. Non-Cryst. Solids 123 (1990) 349–353.

[15] W. Holand, M. Frank, V. Rheinberger, Opalescence in dental products, Thermochim. Acta 280 (1996) 491–499.

[16] T. Yamamuro, L.L. Hench, J. Wilson, T. Yamamuro, L.L. Hench, J. Wilson, Handbook on Bioactive Ceramics, Vol. I: Bioactive Glass and Glass–Ceramics, CRC Press, Boca Raton, FL, 1990.

[17] M.A. Lopes, R.F. Silva, F.J. Monteiro, J.D. Santos, Microstructural dependence of Young's and shear moduli of P_2O_5 glass reinforced hydroxyapatite for biomedical applications, Biomaterials 21 (2000) 749–754.

[18] J. Vogel, P. Wange, P. Hartmann, Phosphate glasses and glass–ceramics for medical applications, Glastech. Ber. Glass Sci. Technol. 70 (1997) 220–223.

[19] G. Rajkumar, S. Aravindan, V. Rajendran, Structural analysis of zirconia-doped calcium phosphate glasses, J. Non-Cryst. Solids 356 (2010) 1432–1438.

[20] M. Navarro, M.P. Ginebra, J. Clément, S. Martínez, G. Avila, J.A. Planell, Physicochemical degradation of titania-stabilized soluble phosphate glasses for medical applications, J. Am. Ceram. Soc. 86 (2003) 1345–1352.

[21] M. Catauro, M.G. Raucci, F.De. Gaetano, M. Marotta, Antibacterial and bioactive silver-containing $Na_2O{\cdot}CaO{\cdot}2SiO_2$ glass prepared by sol–gel method, J. Mater. Sci. Mater. Med. 15 (2004) 831–837.

[22] J.M. Oliveira, R.N. Correia, M.H. Fernandes, Effects of Si speciation on the in vitro bioactivity of glasses, Biomaterials 23 (2002) 371–379.

[23] L.L. Hench, O. Anderson, in: L.L. Hench, J. Wilson (Eds.), An Introduction to Bioceramics, World Scientific, Singapore, 1993, pp. 41–62.

[24] K. Franks, V. Salih, J.C. Knowels, I. Olsen, The effect of MgO on the solubility behavior and cell proliferation in a quaternary soluble phosphate based glass system, J. Mater. Sci. Mater. Med. 13 (2002) 549–556.

[25] T. Kasuga, K. Nagakawa, M. Yoshida, E. Miyade, Compositional dependence of formation of an apatite layer on glass–ceramics in simulated physiological solution, J. Mater. Sci. 22 (1987) 3721–3724.

[26] Y. Ebisawa, T. Kokubo, K. Ohura, T. Yamamuro, Bioactivity of $CaO{\cdot}SiO_2$-based glasses: in vitro evaluation, J. Mater. Sci. Mater. Med. 1 (1990) 239–244.

[27] J.S. Moya, A.P. Tomsia, A. Pazo, C. Santos, F. Guitian, In vitro formation of hydroxylapatite layer in a MgO-containing glass, J. Mater. Sci. Mater. Med. 5 (1994) 529–532.

[28] J.M. Oliveira, R.N. Correia, M.H. Fernandes, Surface modifications of a glass and a glass–ceramic of the MgO–3CaO–P_2O_5–SiO_2 system in a simulated body fluid, Biomaterials 16 (1995) 849–854.

[29] M. Uo, M. Mizuno, Y. Kuboki, A. Makishima, F. Watari, Properties and cytotoxicity of water soluble Na_2O–CaO–P_2O_5 glasses, Biomaterials 19 (1998) 2277–2284.

[30] Baldev Raj, V. Rajendran, P. Palanichamy, Science and Technology of Ultrasonics, Narosa Publication, India, 2004.

[31] P. Palanichamy, P. Kalayanasundram, Baldev Raj, Br. J. Non-destruct. Test. 31 (1989) 78.

[32] Marek Nocuń, Structural studies of phosphate glasses with high ionic conductivity, J. Non-Cryst. Solids 333 (2004) 90–94.

[33] J.A. Sampaio, S.M. Lima, T. Catunda, A.N. Medina, A.C. Bento, M.L. Baesso, Thermal lens versus DTA measurements for glass transition analysis of fluoride glasses, J. Non-Cryst. Solids 304 (2002) 315–321.

[34] A. Oyane, H.-M. Kim, T. Furuya, T. Kokubo, T. Miyazaki, T. Nakamura, Preparation and assessment of revised simulated body fluids, J. Biomed. Mater. Res. 65A (2003) 188–195.

[35] T. Kokubo, H. Takadama, How useful is SBF in predicting in vivo bone bioactivity, Biomaterials 27 (2006) 2907–2915.

[36] C.Q. Ning, Y. Greish, A. El-Ghannam, Crystallization behavior of silica-calcium phosphate biocomposites: XRD and FTIR studies, J. Mater. Sci. Mater. Med. 15 (2004) 1227–1235.

[37] C.Q. Ning, Y. Zhou, In vitro bioactivity of a biocomposite fabricated from HA and Ti powders by powder metallurgy method, Biomaterials 23 (2002) 2909.

[38] F. Branda, R. Fresa, A. Costantini, A. Buri, Bioactivity of $1.25CaO{\cdot}SiO_2$ glass: an FTIR and X-ray study on powdered samples, Biomaterials 17 (1996) 2247–2251.

[39] M. Catauro, M.G. Raucci, F.D.E Gaetano, A. Marotta, Antibacterial and bioactive silver-containing Na_2O–CaO–$2SiO_2$ glass prepared by sol–gel method, J. Mater. Sci. Mater. Med. 15 (2004) 831–837.

[40] C.-P. Chun-Pin Lin, Y.-C. Tseng, F.-H. Lin, J.-D. Liao, W.-H. Lan, Treatment of tooth fracture by medium-energy CO_2 laser and DP-bioactive glass paste: the interaction of enamel and DP-bioactive glass paste during irradiation by CO_2 laser, Biomaterials 22 (2001) 489–496.

[41] S. Kannan, F. Goetz-Neunhoeffer, J. Neubauer, J.M.F. Ferreira, Ionic substitutions in biphasic hydroxyapatite and β-tricalcium phosphate mixtures: structural analysis by rietveld refinement, J. Am. Ceram. Soc. 91 (2008) 1–12.

[42] L. Barbieri, A. Bonamartini Corradi, C. Leonelli, C. Siligardi, T. Manfredini, G. Carlo Pellacani, Effect of TiO_2 addition on the properties of complex aluminosilicate glasses and glass–ceramics, Mater. Res. Bull. 32 (1997) 637–648.

[43] D.S. Brauer, C. Rüssel, J. Kraft, Solubility of glasses in the system P_2O_5–CaO–MgO–Na_2O–TiO_2: experimental and modeling using artificial neural networks, J. Non-Cryst. Solids 353 (2007) 263–270.

[44] V. Rajendran, F.A. Khalifa, H.A. El-Batal, Investigation of acoustical parameters in binary $\times$ Li_2O–$(100 - x)SiO_2$ glasses, Ind. J. Phys. 69A (1995) 237–242.

[45] V. Simon, C. Albon, S. Simon, Silver release from hydroxyapatite self-assembling calcium-phosphate glasses, J. Non-Cryst. Solids 354 (2008) 1751–1755.

[46] K. Franks, I. Abrahams, J.C. Knowels, Development of soluble glasses for biomedical use Part I: *in vitro* solubility measurement, J. Mater. Sci. Mater. Med. 11 (2000) 609–614.

[47] M. Regina, T. Filgueiras, Guy La Torre, L.L. Hench, Solution effects on the surface reactions of three bioactive glass compositions, J. Biomed. Mater. Res. 27 (1993) 1485–1493.

[48] S. Agathopoulos, D.U. Tulyaganov, J.M.G. Ventura, M.A. Karakassides, S. Kannan, J.M.F. Ferreira, Formation of hydroxyapatite onto glasses of the CaO–MgO–SiO_2 system with B_2O_3, Na_2O, CaF_2 and P_2O_5 additives, Biomaterials 27 (2006) 1832–1840.